© 2018. Published by The Company of Biologists Ltd | Journal of Experimental Biology (2018) 221, jeb174912. doi:10.1242/jeb.174912

RESEARCH ARTICLE

Conserved spatio-temporal patterns of suction-feeding flows across aquatic vertebrates: a comparative flow visualization study

Corrine N. Jacobs[1,2,*] and Roi Holzman[1,2]

ABSTRACT

Suction feeding is a widespread prey capture strategy among aquatic vertebrates. It is almost omnipresent across fishes, and has repeatedly evolved in other aquatic vertebrates. By rapidly expanding the mouth cavity, suction feeders generate a fluid flow outside of their mouth, drawing prey inside. Fish and other suction-feeding organisms display remarkable trophic diversity, echoed in the diversity of their skull and mouth morphologies. Yet, it is unclear how variable suction flows are across species, and whether variation in suction flows supports trophic diversity. Using a high-speed flow visualization technique, we characterized the spatio-temporal patterns in the flow fields produced during feeding in 14 species of aquatic suction feeders. We found that suction-feeding hydrodynamics are highly conserved across species. Suction flows affected only a limited volume of ∼1 gape diameter away from the mouth, and peaked around the timing of maximal mouth opening. The magnitude of flow speed increased with increasing mouth diameter and, to a lesser extent, with decreasing time to peak gape opening. Other morphological, kinematic and behavioral variables played a minor role in shaping suction-feeding dynamics. We conclude that the trophic diversity within fishes, and likely other aquatic vertebrates, is not supported by a diversity of mechanisms that modify the characteristics of suction flow. Rather, we suggest that suction feeding supports such trophic diversity owing to the general lack of strong trade-offs with other mechanisms that contribute to prey capture.

KEY WORDS: Particle image velocimetry, Skull kinematics, Fishes

INTRODUCTION

Fish display tremendous trophic diversity, feeding on a vast array of prey types ranging from small drifting zooplankton, algae and detritus to other aquatic vertebrates and hard-shelled prey (Bellwood et al., 2006; Price et al., 2011; Wainwright and Bellwood, 2002). This diversity is reflected in the diversity of their cranial musculature, with species that specialize on small prey characterized by smaller mouths and delicate bones (Price et al., 2011), and species that specialize on hard prey equipped with robust bones and powerful muscles (Price et al., 2011; Stoner and Livingston, 1984). Fish also utilize diverse strategies to capture their prey, often combining protrusion of the mouth towards the prey, forward swimming (ram) and biting (Ferry-Graham et al., 2001; Nemeth, 1997; Wainwright, 2001). In addition, prey capture is almost always aided by the production of suction flows that draw the prey into the mouth (Alexander, 1969; Longo et al., 2016), a mechanism that has also independently evolved in other aquatic vertebrates (Lauder and Shaffer, 1986). Although the diversity in the use of ram, jaw protrusion and (to a lesser extent) biting across aquatic suction feeders is well documented (Ferry-Graham et al., 2001; Lauder and Liem, 1981; Longo et al., 2016; Wainwright et al., 2001), there is little documentation on the variation in suction flows and how these flows have evolved to support the capture of specific prey types.

To capture their prey, fish, and in general aquatic suction feeders, close the distance to their target while opening their mouth and expanding their buccal cavity. The rapid expansion of this cavity, achieved within as little as 5 ms, generates a flow external to the mouth (Day et al., 2015; Higham et al., 2005; Muller et al., 1982). This flow exerts a force on the prey that helps to counter its escape response, dislodge it from its holdfast or transport it into the mouth (Holzman et al., 2007). As such, high suction flow speed and acceleration are considered advantageous for capturing prey (Higham et al., 2006; Holzman et al., 2008a; Osse, 1969; Staab et al., 2012). In general, the dynamics of the flow depend on the volumetric rate of buccal cavity expansion, divided by the area of the mouth aperture (gape), with both changing over time during a prey-acquisition strike (Bishop et al., 2008). The power necessary for this expansion is generated primarily by the axial swimming muscles (the epaxialis and hypaxialis muscles) (Camp et al., 2015). Although Carroll and Wainwright (2009) suggested that suction-feeding performance is constrained by the available muscle power, it is still unclear as to precisely what determines suction feeding performance across fishes.

Because of the technical difficulties associated with measuring flows produced by live animals, much of the research on suction-feeding diversity has focused on surrogates to suction performance. These surrogates include the distance traveled by the prey during a feeding strike (usually normalized to ram; Wainwright, 2001), the pressure produced inside the mouth cavity (Lauder, 1980a; Svanbäck et al., 2002) and the morphological potential to generate this pressure (suction index; Carroll et al., 2004; Wainwright et al., 2007). For example, a comparative study of the distance traveled by the prey during the strike indicated that suction feeding is conserved in comparison with other methods for closing the distance to the prey (i.e. ram and jaw protrusion; Longo et al., 2016). Similarly, the suction index for 30 species of serranid fish was only weakly correlated with strike speed (Oufiero et al., 2012). However, using such surrogates for suction performance does not provide all the functional aspects of suction flows. The distance traveled by the prey is affected by the predator's mouth diameter, the duration of suction flows, and prey size, shape and density (Holzman et al., 2007; Wainwright and Day, 2007). Suction flows are not directly related to buccal pressure, because the shape of the

[1]School of Zoology, Faculty of Life Sciences, Tel Aviv University, Tel Aviv 69978, Israel. [2]The Inter-University Institute for Marine Sciences, POB 469, Eilat 88103, Israel.

*Author for correspondence (corrinej@mail.tau.ac.il)

C.N.J., 0000-0001-8441-9017; R.H., 0000-0002-2334-2551

Received 26 November 2017; Accepted 28 February 2018

cavity and mouth opening dynamics affect the flow produced (Van Wassenbergh et al., 2006a). The suction index does not include behavior and skull kinematics, and also ignores temporal flow patterns, which can be important to prey capture.

However, flow can be visualized and quantitatively analyzed using particle image velocimetry (PIV). PIV consists of seeding the fluid with small neutrally buoyant particles, whose tracking enables quantification of the fluid velocity in the visualized area (Taylor et al., 2014). This technique was used to characterize the suction flows in front of the mouth of four species of ray-finned fishes (*Lepomis macrochirus*, *Micropterus salmoides*, *Danio rerio* and *Carassius auratus*) and one species of elasmobranch (*Chiloscyllium plagiosum*) (Day et al., 2005; Ferry-Graham et al., 2003; Higham et al., 2006; Nauwelaerts et al., 2007, 2008; Pekkan et al., 2016; Staab et al., 2012). The findings revealed that flow speeds at the mouth aperture can reach ∼3 m s^{-1} and accelerations of ∼120 m s^{-2}. However, these extreme flow speeds decayed rapidly as a function of the distance from the mouth: at a distance of ½ gape diameter from the mouth aperture, flow speed was ∼30% of the speed at the mouth center, and at a distance of 1 gape diameter, flow speed was <5% of the speed at the mouth center. Within ray-finned fish, this relationship between flow speed and distance from the mouth was consistent along transects lying at different angles to the centerline within the mid-sagittal and frontal planes (Day et al., 2005, 2015; Ferry-Graham et al., 2003; Holzman and Wainwright, 2009), and generally conformed to the hydrodynamic model suggested by Muller et al. (1982). Therefore, the suction flows are considered radially symmetrical about the mouth. Additionally, flow speed was time-dependent, peaking in *L. macrochirus* and *M. salmoides* around the time of peak gape diameter, but much later in *C. auratus*. Peak flow speed was correlated with the speed of mouth opening in adult *L. macrochirus*, *M. salmoides* and *C. auratus*.

The above-mentioned PIV studies indicate that the spatio-temporal characteristics of suction feeding are hydrodynamically conserved (reviewed by Day et al., 2015). However, it is difficult to generalize this conclusion because of the limited number of species for which PIV data exist. For example, a computational fluid dynamics (CFD) model that quantified the flow in front of the mouth predicted that mouth shape would affect spatial flow patterns (Skorczewski et al., 2012). Specifically, mouths with lateral notches are expected to produce lower flow velocities at the mouth center compared to planar circular mouths (Skorczewski et al., 2012; Van Wassenbergh and Heiss, 2016). However, it is unclear whether the diversity of mouth shapes is reflected in the diversity of suction flows.

The goal of this study was to characterize the diversity of suction-feeding hydrodynamics across aquatic suction-feeding species. We quantified the flow field in front of the mouths of 13 bony fish and one amphibian during suction feeding using PIV. We then quantified peak flow speeds, characterized the decay of flow speed with increasing distance from the mouth, and compared the variation in the temporal patterns of the flow and skull kinematics across species.

MATERIALS AND METHODS

Study organisms

We studied 14 aquatic suction-feeding species, comprising 10 freshwater fishes, three saltwater fishes and one species of aquatic salamander (Figs 1, 2A; Table S1). These species were chosen to represent a diversity of habitats, trophic adaptations and sizes, and are dispersed widely across the vertebrate phylogeny (Fig. 1). Specifically, we planned our sampling to include an ancestral fish with no jaw protrusion, and a derived amphibian with no jaw protrusion or maxillary rotation. We also included three species for which suction-feeding hydrodynamics had been previously published (*L. macrochirus*, *D. rerio* and *C. auratus*).

For each species, one to five adult individuals were used (Table S1). All data were collected using the same methods as in Higham et al. (2005) and Holzman et al. (2008b) to facilitate comparisons among species. We collected new data for 12 species, and re-analyzed raw PIV videos for *L. macrochirus* and *C. auratus* (from Holzman et al., 2008a and Staab et al., 2012, respectively). Freshwater species were purchased through the aquarium trade. Saltwater species were collected locally from the Gulf of Aqaba. Study animals were housed in indoor aquaria and fed daily with a mixture of pellets, *Artemia* (nauplii and adults), blood worms and mysid shrimp, depending on species' preference and prey availability. Study animals were starved for 24 h before filming. Animal maintenance and experimental procedures followed the IACUC approved guidelines at the University of California, Davis, and at the Hebrew University in Jerusalem, which oversees the experiments at the Inter-University Institute in Eilat.

Particle image velocimetry (PIV)

The principles behind PIV are detailed in Raffel et al. (1998) and Taylor et al. (2014) and are explained here in brief. PIV videos for *L. macrochirus* were recorded using the setup described in Holzman et al. (2008a), whereas PIV videos for *C. auratus*, *Ambystoma tigrinum* and *Polypterus endlicheri* were obtained with the setup described in Staab et al. (2012). For all other species, the water was seeded with neutrally buoyant 10 µm hollow glass spheres. An 8 W solid state continuous wave laser (Coherent Genesis MX532-8000, 532 nm, Santa Clara, CA, USA) equipped with a custom-made optical system was used to illuminate the particles. The horizontal laser beam was expanded vertically to form a light sheet <1 mm in thickness and ∼5 cm in height. Videos of prey capture were recorded at 1000 frames s^{-1} using a Photron SA3 high-speed video camera (1 megapixel; Photron, Tokyo, Japan) equipped with 105 mm Nikon lens (f=2.8, Nikon, Tokyo, Japan). In all experiments, the camera was positioned at a right angle to the light sheet, to capture lateral views of the feeding animal. Distances in the videos were scaled by recording an image of a ruler placed in the laser light sheet. Prey were either suspended on a thin wire or released from a feeding tube within the light sheet. Study animals were trained to approach the prey through a gate to ensure that the light sheet was aligned with the sagittal plane of the head. A commercial video camera (Go-pro Hero4, GoPro Inc., San Mateo, CA, USA) was located above the aquarium to verify the position of the animal's mouth with respect to the light sheet, and only sequences in which the two were aligned were used. Over 400 feeding strikes were analyzed for our 14 species (a mean of 15 strikes per individual). Only sequences in which the prey was captured before mouth closing were analyzed.

High-speed PIV video of feeding sequences were saved as avi files and analyzed using MatPIV, a freely available toolbox for analyzing PIV (Holzman et al., 2008a; Staab et al., 2012; Sveen, 2004) in MATLAB (The MathWorks, Natick, MA, USA). MatPIV treats the high-speed video sequence as a series of image pairs, each consisting of two successive frames (at 1 ms intervals). For each image pair, MatPIV estimates the flow speed and direction at each location on a regularly spaced grid of 128×128 cells (16×16 pixels each, with 50% overlap between adjacent cells). The algorithm also calculates a signal-to-noise ratio used to validate the velocity measurements.

Journal of Experimental Biology (2018) 221, jeb174912. doi:10.1242/jeb.174912

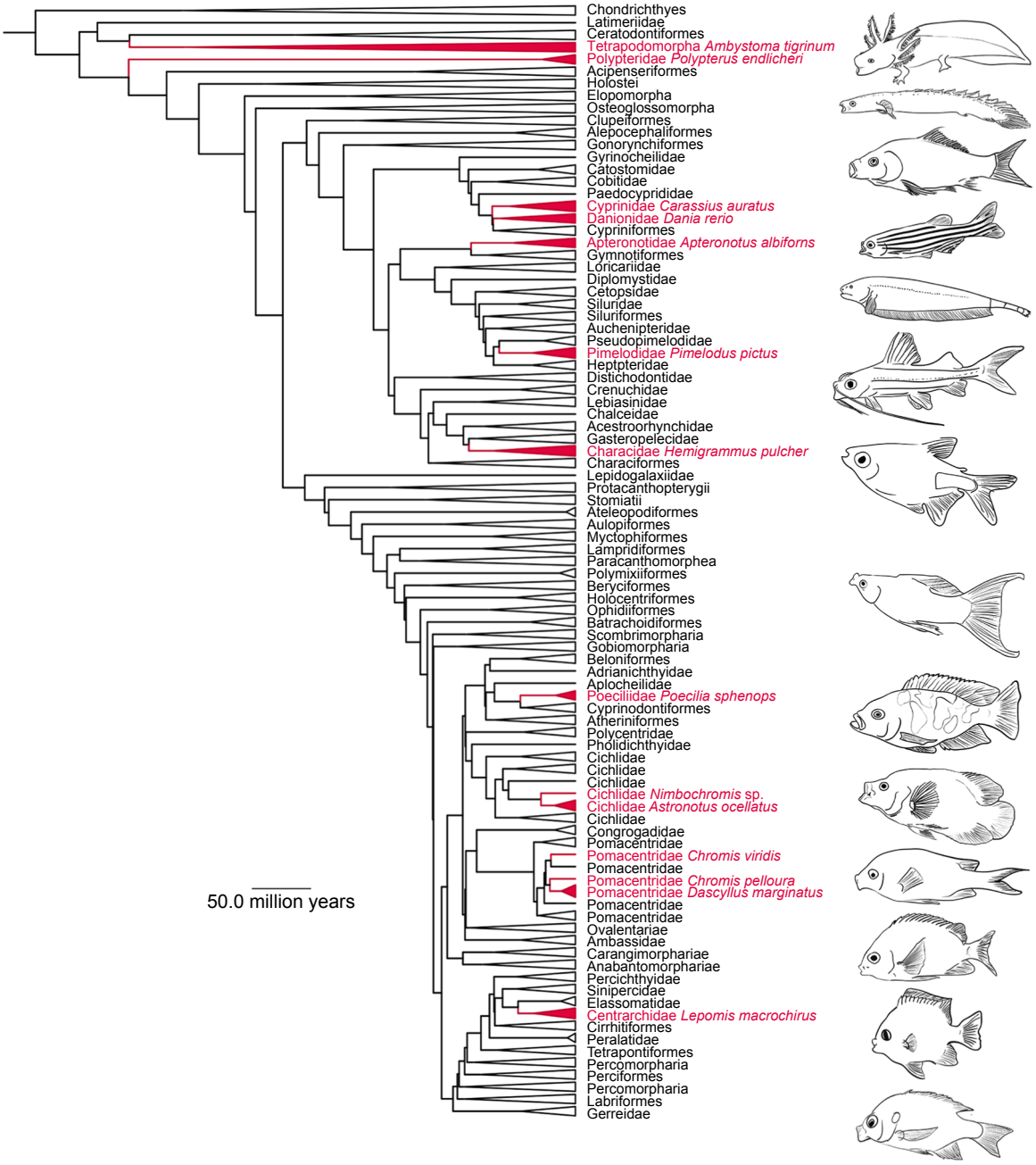

Fig. 1. The phylogenetic placement of the 14 studied species (in red font). Drawings illustrate the diversity in mouth and body morphology during feeding strikes across the studied species, as observed in our videos. The species in drawings correspond to the order in which they appear in the vertebrate's phylogenetic tree (from Betancur-R. et al., 2013). Drawings are not to scale.

To characterize skull kinematics, we digitized in each frame the location of the proximal tip of the upper and lower jaw, the proximal tip of the hyoid bone (when visible), the center of the eye, and the prey's center of mass using DLTdv5 (Hedrick, 2008). From these points, we calculated for each frame the following variables (Oufiero et al., 2012): (1) gape diameter, defined as the distance between the upper and lower jaw points; (2) jaw protrusion distance, defined as the change in distance between mouth center and the eye; and (3) hyoid depression distance, defined as the change in distance between the hyoid bone and the eye point. From the time-dependent patterns of gape diameter, jaw protrusion distance and hyoid depression we determined peak excursions and their respective timings. We defined time to peak gape (TTPG) as the time from when gape diameter first exceeded 20% of its maximal value to the time when it first exceeded 95% of its maximal value. Time to peak jaw protrusion (TTPJP) and hyoid displacement were similarly calculated (Oufiero et al., 2012).

We also measured for each strike the area of the imaginary triangle formed between the projection (on the image) of the upper jaw, lower jaw and the intersection point between the maxilla and lower jaw bones (or skin flaps that are anterior to the bones; Fig. 2B) at the time of peak gape. This area represents the 'notch' that is formed on the lateral side of the mouth when its shape deviates from a planar and near-circular mouth opening (hereafter 'plano-circular'). The 'notch area' was scaled by the area of a circle with a diameter equivalent to gape diameter. We also measured the angle

Journal of Experimental Biology (2018) 221, jeb174912. doi:10.1242/jeb.174912

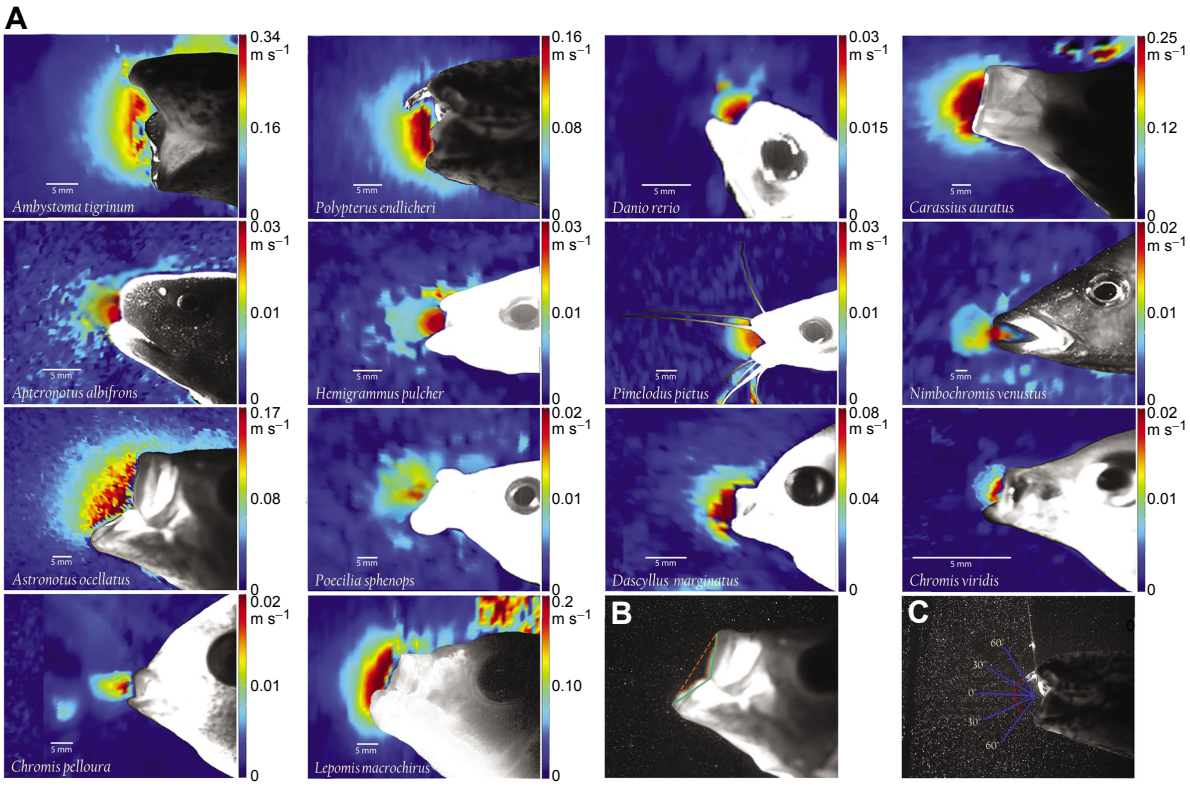

Fig. 2. The diversity of mouth morphology and suction flows across aquatic suction feeders. (A) Images of the 14 studied animals are overlaid over false color images, depicting faster flows as warmer colors and slower flows as cold colors. Because of an order-of-magnitude difference in peak flow speed, each panel has a different velocity scale. (B) The notch area (orange dashed line) is defined as the area of the imaginary triangle formed between the projection of the upper jaw, lower jaw, and the intersection point between the maxilla and lower jaw bones. Notch angle (green lines) is defined as the angle between the maxilla and lower jaw bones. (C) Flow speed for each time frame is measured at 13 points (red x markers) located at a distance of ½ gape distance from the mouth center, separated by 10 deg. The decay of flow speed as a function of the distance from the mouth is characterized based on flow speeds extracted along five transects extending from the mouth center outwards (blue lines).

between the maxilla and lower jaw bones (or skin flaps that are anterior to the bones; hereafter 'notch angle'; Fig. 2B).

Spatio-temporal patterns

To examine the spatial distribution of flow velocities in front of the animal's mouth, we extracted flow speeds along 13 transects that extended anteriorly at different angles from the center of the mouth (Fig. 2C) (Holzman et al., 2008b). The transects extend from the center of the mouth following Day et al. (2015). The centerline transect (0 deg) extended forward parallel to the long axis of the animal's body, from the center of the gape. Twelve additional transects originating from the center of the mouth extended in increments of ±10 deg from the centerline transect. Within each frame, the length of each transect was equivalent to 1.33×gape diameter. Transects were fitted to the mouth at arbitrary time points, but always within the time frame corresponding to 20–95% of peak gape. Flow speed was measured on nine equally spaced points along each transect. Following Day et al. (2005) we scaled the distances to units of gape diameter; flow speeds were scaled to the speed at a distance of ½ gape diameter away from the mouth on the center line. This point was chosen because PIV measurements near solid boundaries are prone to bias because of movements of the animal's body interfering with the signal from the moving particles.

We examined the temporal relationships between flow speed and skull kinematics, focusing on the timing of peak flow speed relative to the timings of peak jaw protrusion, hyoid depression and peak gape diameter. As discussed above, the relationship between flow speed and distance from the mouth is expected to be consistent along transects lying at different angles to the centerline within the mid-sagittal and frontal planes (see Results; Day et al., 2005; Holzman et al., 2008b). We therefore averaged the flow speeds extracted on our 13 transects at a distance of ½ gape diameter from the mouth aperture (hereafter 'flow speed at ½ gape'; Fig. 2C). To account for variation in the timing of kinematic events across and within species, times were scaled to TTPG.

The flux of water flowing into the mouth was calculated as the integral, from the time of mouth opening to closing, of flow speed at the mouth aperture multiplied by gape area. For these calculations, flow speed at the mouth aperture was calculated in the animal-bound frame of reference, i.e. as the sum of ram speed and flow speed at the earthbound frame of reference (Higham et al., 2006). This procedure assumes that the magnitude of flow speed is identical across the mouth orifice, an assumption supported by a CFD model of suction flows (Yaniv et al., 2014) and theory (see discussion in Holzman et al., 2014). We further assume that the mouth is circular (i.e. non-elliptical).

Statistical analyses

To examine the correlation between peak flow speed and skull kinematics, we ran two mixed-effect models with peak flow speed at ½ gape as the dependent variable, and skull kinematic variables as independent variables. The first model included all of the time

Journal of Experimental Biology (2018) 221, jeb174912. doi:10.1242/jeb.174912

variables (TTPG, TTPJP and time to peak hyoid displacement) and distance variables (peak gape diameter, jaw protrusion distance and hyoid displacement), notch area and prey type as independent variables. Time variables were normalized by TTPG and distance variables normalized by peak gape diameter. The other model used speed variables (gape speed, jaw protrusion speed and hyoid depression speed), notch area and prey type as independent variables. Speed variables were normalized by gape speed. This procedure was carried out because of the inter-dependency between speed, distance and time. For both models, species and individuals were treated as random factors. We then compared the 'time+distance' and the 'speed' models using Akaike information criterion (AIC) scores. The best supported model was the 'time+distance' model (ΔAIC<150), and that model is reported hereafter. A similar procedure was used to fit a model that examines the possible correlation between maximal water flux and the above-mentioned parameters, with water flux as the dependent variable, and notch area and 'time+distance' or 'speed' variables as independent variables. Again, the AIC scores were used to choose the best supported model, which was the 'time+distance' model (ΔAIC<280). Note that the hyoid movement could not be quantified in all of the sequences; therefore, only 288 sequences were used in the latter analyses.

Mixed-effect models were run using the lme4 package in R (https://www.r-project.org/), and their *P*-values were obtained by comparing the final model and an intercept-only model using the command 'anova'. R^2 values were calculated using the package MuMin, and *P*-values for the effect of fixed variable were calculated using lmerTest package in R. For each model, both marginal and conditional R^2 values are reported. The marginal R^2 value describes the proportion of variance explained by the fixed factors alone, while the conditional R^2 describes the proportion of variance explained by both the fixed and random factors.

To determine whether the decay of flow speed differed among species, we ran an ANCOVA with (normalized) flow speed along the transects as the dependent variable, and distance from the mouth as a continuous independent variable, with species and transect angle (0, 30 and 60 deg) as factors.

Closely related species are expected to be more similar to one another than expected by chance, violating the assumption of independency required for ANOVA and regression (Díaz-Uriarte and Garland, 1996; Felsenstein, 1985). We tested whether our results were affected by the shared phylogenetic history of our species by repeating the regression analyses using phylogenetic generalized least squares (PGLS) analyses (Blomberg et al., 2016). Unlike our mixed-effect model, PGLS models use species means (rather than all individual data), resulting in a loss of power to detect significant effects. We pruned the time-calibrated tree of Betancur-R. et al. (2013) to highlight the 14 species used in the present study (Fig. 1), and used it to calculate the expected covariance under a Brownian model, which was factored into a GLS model.

To compare the diversity between suction-feeding flows and cranial kinematics, we compared the variance in the species-averaged timing of peak flow speed, peak jaw protrusion and peak hyoid depression using Bartlett's test. A similar test was used to determine whether variance in the species-averaged peak magnitudes of gape speed, flow speed, jaw protrusion speed and hyoid depression speed was homogeneous. When the Bartlett test was significant, we ran a series of *F*-tests to identify which of the variable pairs had significantly different variations. A Bonferroni correction was applied to account for the multiple comparisons.

All the above-mentioned statistical tests were performed using R.

RESULTS

Flow speed and strike kinematics

The gape diameter of the 14 species we measured ranged between 1.4 and 21.4 mm, TTPG between 3 and 189 ms, and jaw protrusion distance between 0 and 18 mm. TTPJP was 1–324 ms, and time to hyoid displacement was 10–253 ms (Table S1). Different species approached the prey differently: some swam towards their prey at a speed of ~0.31 m s^{-1} whereas others swam backwards during a feeding strike at up to ~0.21 m s^{-1} (e.g. *Apteronotus albifrons*). Correspondingly, peak flow speeds at ½ gape distance ranged between ~0.001 and 0.62 m s^{-1}, and the flux of water into the mouth between 3.83×10^{-1} and 3.78×10^{6} m^3 (Figs 2, 3).

A multiple regression mixed-effect model revealed strong correlations between peak flow speed at ½ gape and peak gape diameter, TTPG and normalized TTPJP (marginal and conditional R^2=0.81 and 0.92, respectively; P<0.001; Table 1). Peak flow speed was positively correlated with peak gape diameter (P<0.001; Fig. 3), and negatively correlated with TTPG (P<0.009) and normalized TTPJP (P<0.007). All other timing and distance variables, including notch area and notch angle, had non-significant effects. Peak gape diameter had the largest effect size on peak flow speed, followed by normalized TTPJP and then TTPG (Table 1). The prey type used for the different species was not significantly correlated with flow speed (P>0.3), suggesting that the feeding setup had little effect on the flow field produced and therefore was removed from the final model.

Despite the overall strong positive correlation between gape diameter and peak flow speed, the slopes of the correlation between these variables differed among species (Fig. 3C; Table S2), as was also evident from the difference between the marginal and conditional R^2. Although most species showed a positive correlation, four species (*Nimbochromis venustus*, *Chromis viridis*, *Dascyllus marginatus* and *Pimelodus pictus*) revealed a significant negative correlation between gape diameter and peak flow speed (P<0.05 for all).

The flux of water into the mouth was correlated with peak gape diameter and TTPG (marginal and conditional R^2=0.93 and 0.93, respectively, P<0.001; Table 2). Peak flux was positively correlated with peak gape (P<0.001), and negatively with TTPG (P<0.02). All other timing and distance variables, including notch area and notch angle, had non-significant effects. Peak gape diameter had the largest effect size on water flux, followed by TTPG (Table 2).

Phylogenetically informed analysis

An evolutionarily informed analysis (PGLS) revealed similar correlations (r=0.94) between peak flow speed at ½ gape and the kinematic variables. However, peak gape diameter was the only factor that was found to significantly affect peak flow speed (PGLS P<0.001). Unlike the mixed-effect model, TTPG and normalized TTPJP did not significantly affect peak flow speed. Similarly, a PGLS analysis revealed high correlations (r=0.98) between water flux and the kinematic variables, with a significant positive effect only for peak gape diameter (PGLS P<0.001). Other kinematic variables had non-significant effects on both maximal flow speed and water flux.

Spatial flow patterns

The decay of flow speed in front of the mouth closely followed that postulated by Muller et al. (1982) for flow decay on the centerline. Flow speed decayed rapidly with increasing distance from the mouth (Figs 2, 4; Fig. S1). An ANCOVA test (R^2=0.97, P<0.001) revealed that the decay did not significantly differ between transects laid at different angles (P>0.9 and P>0.32 for 0 versus 30 deg and 0 versus 60 deg, respectively). Furthermore, none of the interaction

Journal of Experimental Biology (2018) 221, jeb174912. doi:10.1242/jeb.174912

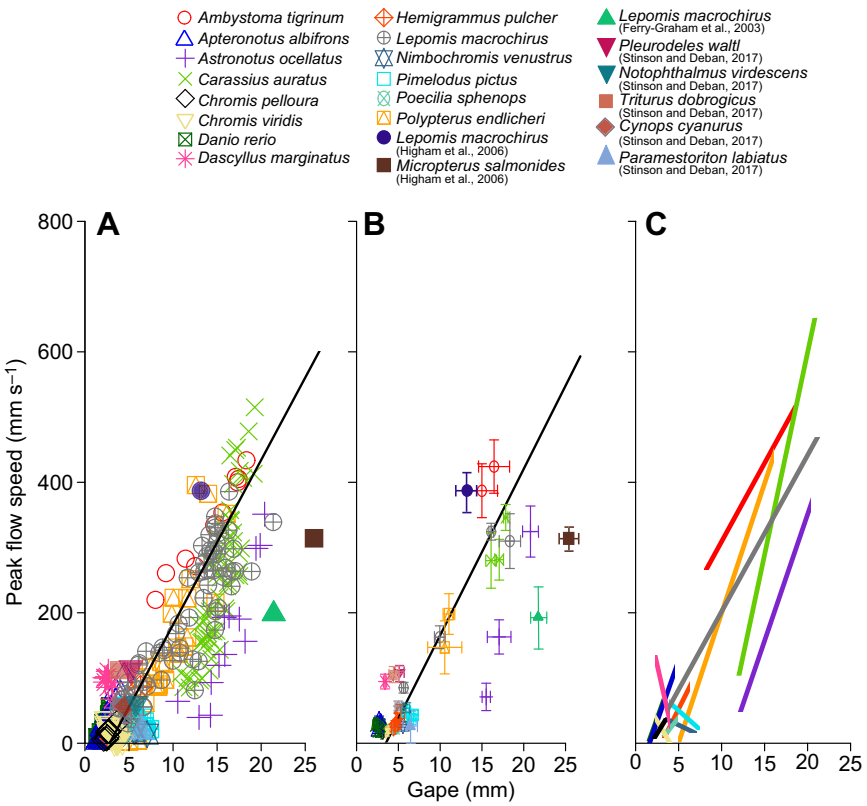

Fig. 3. Scaling of peak flow speed across species. Peak flow speed at a distance of ½ gape diameter away from the mouth center is plotted against peak gape diameter. Colors depict different species. (A) All 403 analyzed feeding strikes including two species from Higham et al. (2006), one species from Ferry-Graham et al. (2003) and five species of salamander from Stinson and Deban (2017). (B) Individual means and two species from Higham et al. (2006), one species from Ferry-Graham et al. (2003) and five species of salamander from Stinson and Deban (2017) (±s.e.). The regression lines in A and B are from the mixed effect model (Peak flow speed=19.37×Gape diameter–37.61; marginal R^2=0.81, P<0.001). (C) The regression lines between peak flow speed and peak gape diameter, calculated separately for each species (R^2>0.57 and P<0.05 for all regressions).

terms between transect angle and species were significant (P>0.05 for all), indicating that, across species, the decay of flow speed with increasing distance from the mouth was consistent along transects lying at different angles to the centerline within the mid-sagittal plane (Figs 2C, 4). The slope of the flow decay differed among species, with a significantly steeper decay in *Chromis pelloura*, *Chromis viridis*, *Hemigrammus pulcher*, *Poecilia sphenops* and *Nimbochromis venustus* (as indicated by a significant interaction term between species and the distance from the mouth). However, these differences in slopes corresponded to small differences in spatial flow patterns (Table S2). For example, the mean distance at which flow speed was equivalent to 20% of the speed at ½ gape distance was 0.94 gape diameters, whereas the distance for the same flow speed in *C. pelloura* (which had the steepest decay) was 0.89 gape diameters. The slope of the decay was not correlated to the notch area (linear regression, P>0.05, R^2=0.05; Fig. 5) or notch angle (linear regression, P>0.09, R^2=0.06).

Table 1. ANOVA results for mixed effect model describing the effects of kinematic variables on peak flow speed

Variable	Effect size	MS	*F*	Pr(>*F*)
Max. gape diameter (mm)	1.068	40.402	380.74	<2.2e–16***
Time to peak gape (s)	–0.069	0.746	7.03	0.0084**
Normalized time to peak flow (mm s^{-1})	–0.023	0.119	1.12	0.2906
Jaw protrusion distance (mm)	0.021	0.064	0.61	0.4363
Normalized time to peak jaw protrusion (s)	–0.066	0.810	7.63	0.0061**
Hyoid depression distance (mm)	0.042	0.321	3.03	0.0835
Normalized time to peak hyoid depression (s)	–0.020	0.074	0.69	0.4058
Ram speed (mm s^{-1})	0.029	0.163	1.54	0.2165
Angle of mouth notch (deg)	0.003	0.001	0.01	0.9331
Area of mouth notch (mm)	0.019	0.040	0.37	0.5409

P-values are calculated using Satterthwaite approximation for degrees of freedom (Satterthwaite, 1946). ***P<0.001; **P<0.01.

Temporal flow patterns

Overall, the time of peak flow speed closely corresponded to the time of peak gape. Across species, peak flow speed occurred at 0.67–1.53 TTPG cycles. The salamander *Ambysoma tigrinum*

Table 2. ANOVA results for mixed-effect model describing the effects of kinematic variables on water flux

Variable	Effect size	MS	*F*	Pr(>*F*)
Max. gape diameter (mm)	0.979	131.186	1923.93	<9.0e–14***
Time to peak gape (s)	–0.044	0.443	6.49	0.0132*
Normalized time to peak flow (mm s^{-1})	–0.020	0.099	1.45	0.2298
Jaw protrusion distance (mm)	–0.003	0.003	0.04	0.8355
Normalized time to peak jaw protrusion (s)	–0.015	0.047	0.69	0.4058
Hyoid depression distance (mm)	–0.001	0.008	0.11	0.7381
Normalized time to peak hyoid depression (s)	–0.020	0.084	1.23	0.2678
Ram speed (mm s^{-1})	0.004	0.004	0.06	0.8108
Angle of mouth notch (deg)	–0.008	0.008	0.11	0.7411
Area of mouth notch (mm)	0.000	0.000	0.00	0.9930

P-values are calculated using Satterthwaite approximation for degrees of freedom (Satterthwaite, 1946). ***P<0.001; *P<0.05.

Journal of Experimental Biology (2018) 221, jeb174912. doi:10.1242/jeb.174912

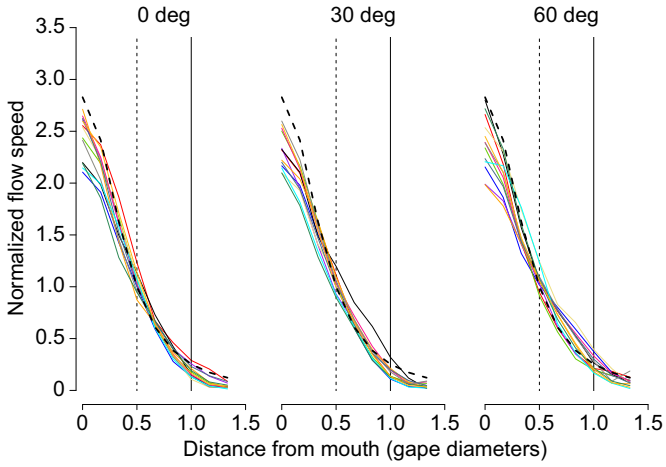

Fig. 4. The decay of flow speed as a function of distance from the center of the mouth aperture on the 0, 30 and 60 deg transects. Flow speed was normalized to the flow speed at a distance of ½ gape diameter from the mouth center. Distance (*x*-axis) is in units of gape diameters. Different colors represent different species (see Fig. 3). Flow was measured on nine equally spaced points along each transect. The thick dashed black line represents the decay of flow speed expected based on the model of Muller et al. (1982). Vertical dashed and solid lines depict the distances of 0.5 and 1.0 gape diameters from the mouth center, respectively.

exhibited the earliest peak flow speed while the goldfish *C. auratus* exhibited the latest. The time of peak flow speed for all other species was 0.91–1.28 TTPG cycles. We used a Bartlett test to compare the variance in the timing of three kinematic events (timing of peak flow speed, jaw protrusion and hyoid displacement). The results indicated a significant deviation from homogeneity of variance (Bartlett's K^2=14.438, P<0.001; Fig. 6). The variance in the timing of peak flow speed (s.d.=0.19) was significantly less than the variance in TTPJP (s.d.=0.62; F-test, P<0.001) and time to peak hyoid depression (s.d.=0.54; F-test, P<0.001; all in units of TTPG cycles).

We also used the Bartlett test to compare the variance in magnitude (mm s^{-1}) of four kinematic variables (magnitude of peak flow, jaw protrusion, hyoid displacement and gape speed). The results indicated a significant deviation from homogeneity of variance (Bartlett's K^2=8.57, P<0.036). However, the only significant pair-wise difference was between the variance in flow speed (s.d.=7.57 mm s^{-1}) and jaw protrusion speed (s.d.=17.37 mm s^{-1}).

DISCUSSION

The species examined in the present study encompass diverse characteristic diets and a broad diversity in their mouth morphology and ability to protrude their jaws (Figs 1, 2, Table 1; Fig. S1). In addition, these species exhibited considerable behavioral diversity, as reflected in the variation in timing of kinematic events (Fig. 6). All, however, use suction feeding as part of their prey capture technique. Based on the morphological and behavioral diversity, we expected variation in the spatio-temporal patterns of flow speed, as well as in the magnitude of peak flow speed and the volumetric flux of water entering the mouth during a feeding strike. However, our results indicate that the key features of suction-feeding hydrodynamics are highly conserved across suction feeders (Fig. 2; Fig. S1).

Determinants of suction performance

Within our studied species, suction performance was affected, by and large, by the size of the mouth, with other morphological and behavioral traits having a minor effect on suction flow. This pattern could be the result of scaling of the volume of the buccal cavity and gape diameter. Suction flow speed at the mouth is determined by the instantaneous rate of volumetric expansion of the buccal cavity, divided by the (instantaneous) gape area. Under isometric growth, buccal volume should increase with gape diameter to the third power (gape^3), whereas gape area should scale with gape^2. Under this simplified scaling argument, flow speed is expected to scale with gape diameter. The effect of TTPG in our multiple regression model reflects the importance of the time required to expand the buccal cavity within an individual fish, and demonstrates that variations in this time impacts peak flow velocity. However, the effect size of TTPG was much lower than that of gape size (Table 1), leading to the overall dominant effect of gape diameter on the magnitude of flow speed. Our data did not reveal a significant correlation between gape diameter and TTPG. Because our species represent a broad sampling of Osteichthyes and amphibian species, we consider this finding as representing the general trend within fishes and amphibians. However, deviations from isometric growth are certainly possible (Van Wassenbergh et al., 2006b). Interestingly, Carroll and Wainwright (2009) predicted that suction feeding is limited by the available muscle power. If this hypothesis is true, suction power should scale with gape diameter.

Mechanisms supporting trophic diversity

Our analysis of the spatio-temporal patterns of suction flow, and of the variables that determine flow speed and flux, indicate that

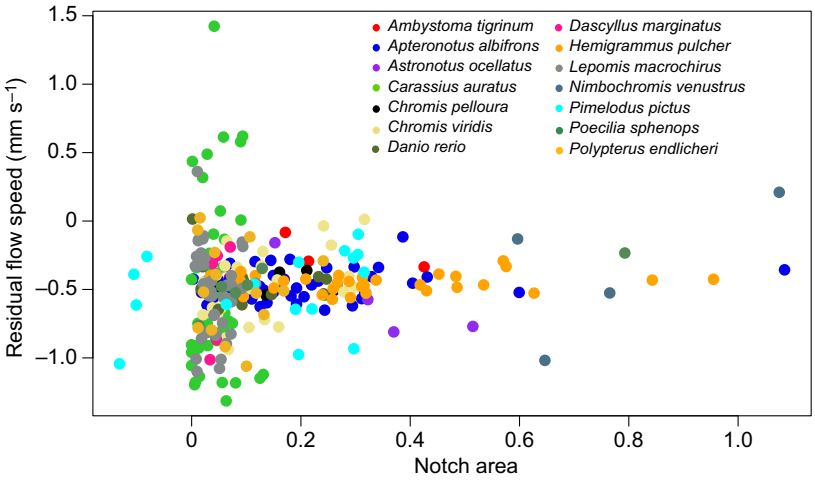

Fig. 5. The partial effect of notch area on flow speed. This is shown as the residual flow speed from the mixed effect model against the normalized notch area. Negative notch area represents a convex mouth opening.

Journal of Experimental Biology (2018) 221, jeb174912. doi:10.1242/jeb.174912

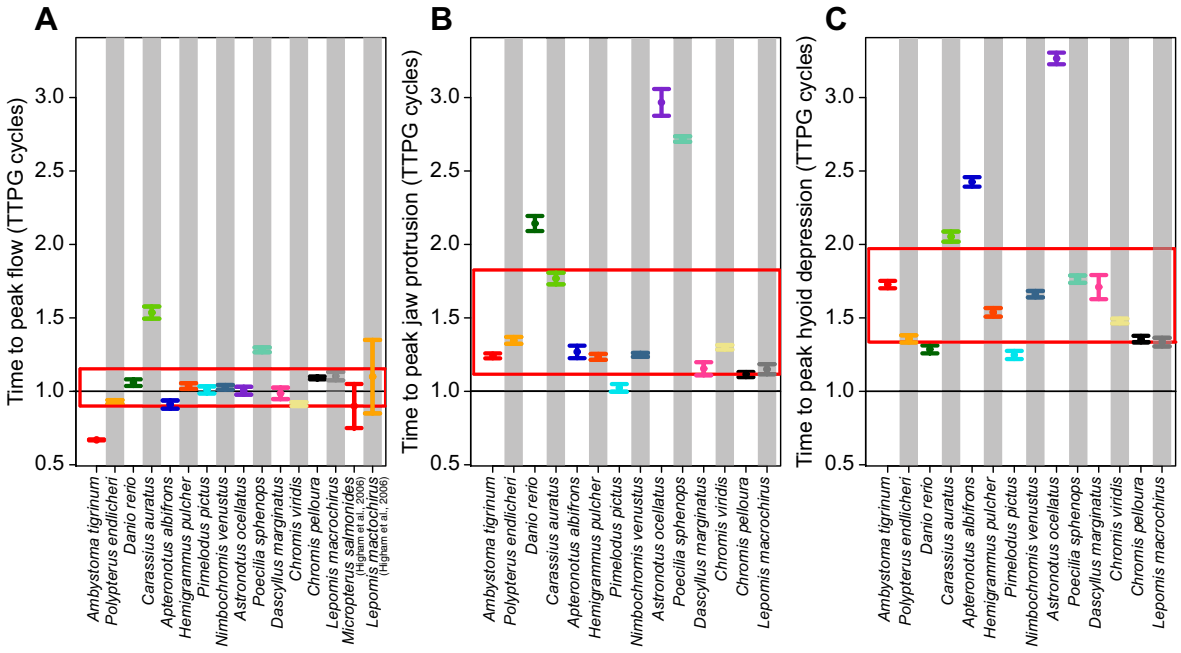

Fig. 6. Variation in the timing of flow and strike kinematics during feeding strikes across species. Diversity in the timing of (A) peak flow speed with two added species (Higham et al., 2006), (B) jaw protrusion and (C) hyoid displacement. Data are the mean±s.d. timing of peak events, in units of TTPG cycles. For example, a value of 1 is achieved when peak flow speed co-occurs with TTPG, and a value of 1.5 is expected when peak flow speed occurs after peak gape, at a time interval equaling half of the TTPG of that strike. The red box in each panel depicts the 95% confidence interval for all our individuals.

suction feeding is a conserved, highly stereotypical behavior. These findings suggest that the trophic diversity within fishes and suction-feeding amphibians is not supported by a diversity of mechanisms that modify the characteristics of suction flow. Rather, we suggest that suction feeding supports the trophic diversity within fishes and suction-feeding amphibians because of the general lack of a strong trade-off with other mechanisms that contribute to prey capture, and because suction performance is tightly correlated with gape diameter. This is ecologically relevant, as body size (generally correlated with gape size within fish; Werner, 1974) is considered a major biological variable affecting multiple ecological functions, including reproductive output (Trippel et al., 1997), vulnerability to predation and access to food resources (Zaret and Kerfoot, 1975), and mating opportunities (Cargnelli and Gross, 1996), among other fitness-determining functions. In fish, body size is correlated to trophic level (Romanuk et al., 2011), implying that linear growth can broaden the range of available food recourses. This is evident as body size offers a good interpretation of the ordering of animal species as assumed in the cascade model, a stochastic model of food web structure (Cohen et al., 1993; Pauly et al., 1998). Additionally, body size is considered a labile trait within vertebrates (Elliot and Hurley, 1995; Jobling, 1983).

Our results suggest a lack of trade-off between suction flow and jaw protrusion, and that the timing of flow speed is independent of other cranial motions, allowing kinematic flexibility (Fig. 6) without impairing suction performance. This has been similarly suggested by Longo et al. (2016), who quantified the distance covered by the prey, the fish body and the jaws during suction feeding. Our results also support the lack of a trade-off between suction feeding and biting ability (Longo et al., 2016; Van Wassenbergh et al., 2007), as species that tend to bite or pick-and-grab their prey (e.g. *Poecilia sphenops*, *Hemigrammus pulcher* and *Pimelodus pictus*) did not differ in their suction performance from other trophic groups. Although under our experimental conditions ram speed did not correlate with suction flow speed, Longo et al. (2016) reported a trade-off between the distance covered owing to body ram and the prey movement owing to suction flow. In contrast, ram speed and gape size (which, according to our results, scales with flow speed) exhibited a positive relationship in cichlids (Higham et al., 2007) but were not correlated in serranids (Oufiero et al., 2012). Because negative, positive and neutral correlations were found to describe the relationship between ram speed and suction flow or its surrogates, it is difficult to generalize a strong trade-off between ram and suction flow speeds.

One of the major advances in the history of ray-finned fish is the evolution of the maxillary rotation and upper jaw protrusion (Lauder, 1985; Westneat, 2005). When the upper jaw is fused to the skull (e.g. in *Polypterus endlicher* and *Ambystoma tigrinum*) and in the absence of maxillary rotation or soft tissue blocking the gap between the jaws (a skin flap), a 'notch' can be formed at each side of the mouth. This notch has been considered disadvantageous because water can flow through it, reducing the flow speed directly in front of the mouth and altering the spatial patterns of the flow. A CFD model that examined the effect of the notch on the characteristics of suction flows predicted an ∼37% loss in flow speed in front of the mouth aperture for the case of a notched mouth compared with a plano-circular one (Skorczewski et al., 2012). Similarly, a CFD model of aquatic and terrestrial newts with different notch areas postulated that decreasing the notch area would increase flow speed in front of the mouth by ∼30% (Van Wassenbergh and Heiss, 2016). Our results, however, do not support these predictions. Our mixed effect multiple regression model indicated a non-significant effect of the notch area (or angle) on the peak magnitude of flow speed in front of the mouth (Table 1, Fig. 5). In addition, the notch area (or angle) was not correlated with the slope of flow decay in front of the mouth or with the distance from the mouth at which detectable suction flows still occur. Although the changes to the spatial patterns of the flow field in the

mid-sagittal plane (i.e. slope of decay) can be small (<10%) and therefore potentially undetectable given the variance in measured parameters (Van Wassenbergh and Heiss, 2016), the effect of notch area on flow speed at the mouth center is expected to be substantial (>25%). Van Wassenbergh and Heiss (2016) demonstrated that the patterns of hyoid depression can compensate for a larger notched area. It is thus possible that the different cranial kinematics of our different species mask the effect of the notched area, leading to an overall lack of notch effect on flow speed.

Our results further indicate the lack of a functional trade-off between jaw protrusion and the ability to generate fast suction flows. Jaw protrusion distance and speed were not correlated with maximal flow speeds across our studied species. Normalized time to peak jaw protrusion was negatively correlated with the magnitude of peak flow speed (i.e. faster flows were associated with a closer temporal occurrence of peak gape and peak jaw protrusion); however, the effect size was low. Both faster flow speeds (Wainwright and Day, 2007) and faster jaw protrusion (Holzman et al., 2008a) contribute to feeding success by increasing the hydrodynamic force that draws the prey into the mouth. Thus, the lack of a trade-off between jaw protrusion and the ability to generate fast suction flows suggest that the two mechanisms can independently evolve to increase feeding success. Such a scenario of several traits that contribute independently to performance has been suggested to mitigate evolutionary trade-offs and increase functional diversity (Holzman et al., 2011).

Comparison with previous studies

In all our studied species, suction flows exhibited a consistent decay with increasing distance from the mouth along transects lying at different angles to the centerline within the mid-sagittal plane (Figs 2C, 4). We interpret this consistency as indicating that water is drawn in from a 'mushroom-shaped' volume around the mouth (Fig. 2A), with water from both above and below the mouth being moved towards the mouth. This pattern leads to a rapid drop in flow speed away from the mouth (Fig. 4). Across our study species, the flow speed at a distance of ∼1 gape diameter away from the mouth was ∼5±3% (mean±s.d) of the flow at the center of the mouth orifice (range 0.02–0.38 mm s^{-1}). These flow patterns are in agreement with results from hydrodynamic modeling (Lauder, 1980b; Muller et al., 1982; Van Wassenbergh and Aerts, 2009; Van Wassenbergh et al., 2006a; Weihs, 1980; Yaniv et al., 2014). Furthermore, examination of fluid flow fields obtained in flow visualization studies of ray-finned fish, elasmobranchs and other suction-feeding vertebrates confirms the generality of this pattern, at least when feeding away from the substrate (Day et al., 2005; Ferry-Graham et al., 2003; Higham et al., 2006; Lauder and Clark, 1984; Nauwelaerts et al., 2007, 2008; Pekkan et al., 2016; Staab et al., 2012; Stinson and Deban, 2017). Thus, suction feeding is effective only when the prey is very close to the mouth, and it is not surprising that other mechanisms for rapidly closing the distance to the prey (e.g. body and jaw ram) are important for aquatic suction feeding. However, for a prey located inside the flow field, the force exerted by the suction flows hinders its ability to escape the predator (Stewart et al., 2013).

Unfortunately, only a few flow visualization studies report both peak flow speed and mouth size (Ferry-Graham et al., 2003; Higham et al., 2006; Stinson and Deban, 2017). However, the strong effect of gape size on peak flow speed observed in our study remains highly consistent with the data from those reports. We used species means of gape size and peak flow speed from those studies and from our dataset, and calculated the regression coefficient between the gape size and flow speed. Where necessary, we evaluated the flow speed at ½ gape diameter from the mouth based on the stereotypic flow decay reported above. The regression coefficient remained consistently high (R^2=0.8 for our data, R^2=0.68 with species means from above-mentioned studies) despite the different methods used to evaluate flow speed and gape diameter.

Species-specific deviations from the above patterns

By measuring multiple parameters that could influence the flow produced during suction feeding, we were able to determine that maximum gape diameter, TTPG and normalized TTPJP are the only factors to significantly influence the speed of the suction flow. Thus, the larger the mouth diameter and the faster a suction feeder can open its mouth to its full potential, the faster the flow speed will be. However, for four species we found a negative correlation between flow speed and gape diameter. This pattern can be explained by the fact that, in these species, the flux of the water into the mouth is not correlated with gape diameter. In other words, in these species, the same volume of water is drawn through a larger orifice, leading to slower flow at the mouth.

Across our species, the time of peak flow speed closely corresponded to the time of peak gape. Most of our studied species exhibited a tight coupling of the timing of peak gape and flow speed, with peak flow speed occurring within ±0.1 gape cycles from the time of peak gape. Surprisingly, there was no correlation (r=0.05) between the normalized timing of peak flow speed and peak hyoid displacement. The salamander *A. tigrinum* exhibited an extremely early peak flow speed (0.67 TTPG cycles), which could be related to the lack of opercular bones, and consequently to the salamander's inability to modulate the pressure in its opercular cavity (Lauder, 1980b; van Leeuwen and Muller, 1984). Other species revealing extreme timings (falling outside the 95% CI for our species) were the goldfish *C. auratus* (1.56 TTPG cycles) and *P. sphenops* (1.28 TTPG cycles). Both species are pick-and-grab feeders, and it is possible that suction plays only a minor role in prey capture and is delayed in order to help with prey sifting or transporting prey into the mouth. However, the biomechanical basis of the delayed flows is unclear, and understanding this requires tracking of the internal skull kinematics.

Acknowledgements

The authors thank N. Paz for editorial assistance.

Competing interests

The authors declare no competing or financial interests.

Author contributions

Conceptualization: C.N.J., R.H.; Methodology: C.N.J., R.H.; Software: C.N.J., R.H.; Validation: C.N.J., R.H.; Formal analysis: C.N.J., R.H.; Investigation: C.N.J., R.H.; Resources: C.N.J., R.H.; Data curation: C.N.J., R.H.; Writing - original draft: C.N.J., R.H.; Writing - review & editing: C.N.J., R.H.; Visualization: C.N.J., R.H.; Supervision: R.H.; Project administration: C.N.J., R.H.; Funding acquisition: R.H.

Funding

The study was funded by Israel Science Foundation grant 965/15 to R.H. C.N.J. thanks Center for Life in the Flow for financial support.

Data availability

Data are available from figshare (Jacobs and Holzman, 2018): https://doi.org/10.6084/m9.figshare.5923114.

Supplementary information

Supplementary information available online at http://jeb.biologists.org/lookup/doi/10.1242/jeb.174912.supplemental

References

Alexander, R. M. N. (1969). Mechanics of the feeding action of a cyprinid fish. *J. Zool.* **159**, 1-15.

Bellwood, D. R., Wainwright, P. C., Fulton, C. J. and Hoey, A. S. (2006). Functional versatility supports coral reef biodiversity. *Proc. R. Soc. B Biol. Sci.* **273**, 101-107.
Betancur-R, R., Broughton, R. E., Wiley, E. O., Carpenter, K., López, J. A., Li, C., Holcroft, N. I., Arcila, D., Sanciangco, M., Cureton, J. C.II. et al. (2013). The tree of life and a new classification of bony fishes. *PLoS Curr.* **5**, 1-28.
Bishop, K. L., Wainwright, P. C. and Holzman, R. (2008). Anterior-to-posterior wave of buccal expansion in suction feeding fishes is critical for optimizing fluid flow velocity profile. *J. R. Soc. Interface* **5**, 1309-1316.
Blomberg, S. P., Lefevre, J. G., Wells, J. A. and Waterhouse, M. (2016). Independent contrasts and PGLS regression estimators are equivalent. *Syst. Biol.* **61**, 382-391.
Camp, A. L., Roberts, T. J. and Brainerd, E. L. (2015). Swimming muscles power suction feeding in largemouth bass. *Proc. Natl. Acad. Sci. USA* **112**, 8690-8695.
Cargnelli, L. M. and Gross, M. R. (1996). The temporal dimension in fish recruitment: birth date, body size, and size-dependent survival in a sunfish (bluegill: *Lepomis macrochirus*). *Can. J. Fish. Aquat. Sci.* **53**, 360-367.
Carroll, A. M. and Wainwright, P. C. (2009). Energetic limitations on suction feeding performance in centrarchid fishes. *J. Exp. Biol.* **212**, 3241-3251.
Carroll, A. M., Wainwright, P. C., Huskey, S. H., Collar, D. C. and Turingan, R. G. (2004). Morphology predicts suction feeding performance in centrarchid fishes. *J. Exp. Biol.* **207**, 3873-3881.
Cohen, J. E., Pimm, S. L., Yodzis, P. and Saldana, J. (1993). Body sizes of animal predators and animal prey in food webs. *J. Anim. Ecol.* **62**, 67-78.
Day, S. W., Higham, T. E., Cheer, A. Y. and Wainwright, P. C. (2005). Spatial and temporal patterns of water flow generated by suction-feeding bluegill sunfish *Lepomis macrochirus* resolved by particle image velocimetry. *J. Exp. Biol.* **208**, 2661-2671.
Day, S. W., Higham, T. E., Holzman, R. and Van Wassenbergh, S. (2015). Morphology, kinematics, and dynamics: the mechanics of suction feeding in fishes. *Integr. Comp. Biol.* **55**, 21-35.
Díaz-Uriarte, R. and Garland, T. (1996). Testing hypotheses of correlated evolution using phylogenetically independent contrasts: sensitivity to deviations from Brownian motion. *Syst. Biol.* **45**, 27-47.
Elliot, J. M. and Hurley, M. A. (1995). The functional relationship between body size and growth rate in fish. *Funct. Ecol.* **9**, 625-627.
Felsenstein, J. (1985). Phylogenies and the comparative method. *Am. Nat.* **125**, 1-15.
Ferry-Graham, L. A., Wainwright, P. C., Westneat, M. W. and Bellwood, D. R. (2001). Modulation of prey capture kinematics in the cheeklined wrasse *Oxycheilinus digrammus* (Teleostei: Labridae). *J. Exp. Zool.* **290**, 88-100.
Ferry-Graham, L. A., Wainwright, P. C. and Lauder, G. V. (2003). Quantification of flow during suction feeding in bluegill sunfish. *Zoology* **106**, 159-168.
Hedrick, T. L. (2008). Software techniques for two- and three-dimensional kinematic measurements of biological and biomimetic systems. *Bioinspir. Biomim.* 3, 1-7.
Higham, T. E., Day, S. W. and Wainwright, P. C. (2005). Sucking while swimming: evaluating the effects of ram speed on suction generation in bluegill sunfish *Lepomis macrochirus* using digital particle image velocimetry. *J. Exp. Biol.* **208**, 2653-2660.
Higham, T. E., Day, S. W. and Wainwright, P. C. (2006). Multidimensional analysis of suction feeding performance in fishes: fluid speed, acceleration, strike accuracy and the ingested volume of water. *J. Exp. Biol.* **209**, 2713-2725.
Higham, T. E., Hulsey, C. D., Říčan, O. and Carroll, A. M. (2007). Feeding with speed: prey capture evolution in cichilds. *J. Evol. Biol.* **20**, 70-78.
Holzman, R. and Wainwright, P. C. (2009). How to surprise a copepod: strike kinematics reduce hydrodynamic disturbance and increase stealth of suction-feeding fish. *Limnol. Oceanogr.* **54**, 2201-2212.
Holzman, R., Day, S. W. and Wainwright, P. C. (2007). Timing is everything: coordination of strike kinematics affects the force exerted by suction feeding fish on attached prey. *J. Exp. Biol.* **210**, 3328-3336.
Holzman, R., Day, S. W., Mehta, R. S. and Wainwright, P. C. (2008a). Jaw protrusion enhances forces exerted on prey by suction feeding fishes. *J. R. Soc. Interface* **5**, 1445-1457.
Holzman, R., Collar, D. C., Day, S. W., Bishop, K. L. and Wainwright, P. C. (2008b). Scaling of suction-induced flows in bluegill: morphological and kinematic predictors for the ontogeny of feeding performance. *J. Exp. Biol.* **211**, 2658-2668.
Holzman, R., Collar, D. C., Mehta, R. S. and Wainwright, P. C. (2011). Functional complexity can mitigate performance trade-offs. *Am. Nat.* **177**, E69-E83.
Holzman, R., Perkol-Finkel, S. and Zilman, G. (2014). Mexican blind cavefish use mouth suction to detect obstacles. *J. Exp. Biol.* **217**, 1955-1962.
Jacobs, C. and Holzman, R. (2018). Suction feeding kinematic data for 14 aquatic species. *figshare* https://doi.org/10.6084/m9.figshare.5923114
Jobling, M. (1983). Growth studies with fish-overcoming the problems of size variation. *J. Fish Biol.* **22**, 153-157.
Lauder, G. V. (1980a). The suction feeding mechanism in sunfishes (*Lepomis*): an experimental analysis. *J. Exp. Biol.* **88**, 49-72.
Lauder, G. V. (1980b). Hydrodynamics of prey capture by teleost fishes. In *Biofluid Mechanics* (ed. D. J. Schneck), pp. 161-181. Boston, MA: Springer.
Lauder, G. V. (1985). Functional morphology of the feeding mechanism in lower vertebrates. *Vertebr. Morphol.* **30**, 179-188.
Lauder, G. V. and Clark, B. D. (1984). Water flow patterns during prey capture by teleost fishes. *J. Exp. Biol.* **113**, 143-150.
Lauder, G. V. and Liem, K. F. (1981). Prey capture by *Luciocephalus pulcher*: implications for models of jaw protrusion in teleost fishes. *Environ. Biol. Fishes* **6**, 257-268.
Lauder, G. V. and Shaffer, H. B. (1986). Functional design of the feeding mechanism in lower vertebrates: unidirectional and bidirectional flow systems in the tiger salamander. *Zool. J. Linn. Soc.* **88**, 277-290.
Longo, S., McGee, M. D., Oufiero, C. E., Waltzek, T. B. and Wainwright, P. C. (2016). Body ram, not suction, is the primary axis of suction-feeding diversity in spiny-rayed fishes. *J. Exp. Biol.* **219**, 119-128.
Muller, M., Osse, J. W. M. and Verhagen, J. H. G. (1982). A quantitative hydrodynamical model of suction feeding in fish. *J. Theor. Biol.* **95**, 49-79.
Nauwelaerts, S., Wilga, C., Sanford, C. and Lauder, G. V. (2007). Hydrodynamics of prey capture in sharks: effects of substrate. *J. R. Soc. Interface* **4**, 341-345.
Nauwelaerts, S., Wilga, C. D., Lauder, G. V. and Sanford, C. P. (2008). Fluid dynamics of feeding behaviour in white-spotted bamboo sharks. *J. Exp. Biol.* **211**, 3095-3102.
Nemeth, D. H. (1997). Modulation of attack behavior and its effect on feeding performance in a trophic generalist fish, *Hexagrammos decagrammus*. *J. Exp. Biol.* **2164**, 2155-2164.
Osse, J. W. M. (1969). Functional morphology of the head of the perch (*Perca fluviatilis* L.): an electromyographic study. *Netherlands J. Zool.* **19**, 289-392.
Oufiero, C. E., Holzman, R., Young, F. A. and Wainwright, P. C. (2012). New insights from serranid fishes on the role of trade-offs in suction-feeding diversification. *J. Exp. Biol.* **215**, 3845-3855.
Pauly, D., Christensen, V., Dalsgaard, J., Froese, R. and Torres, F. Jr. (1998). Fishing down marine food webs. *Science (80-.)* **279**, 860-863.
Pekkan, K., Chang, B., Uslu, F., Mani, K., Chen, C.-Y. and Holzman, R. (2016). Characterization of zebrafish larvae suction feeding flow using μPIV and optical coherence tomography. *Exp. Fluids* **57**, 105-112.
Price, S. A., Holzman, R., Near, T. J. and Wainwright, P. C. (2011). Coral reefs promote the evolution of morphological diversity and ecological novelty in labrid fishes. *Ecol. Lett.* **14**, 462-469.
Raffel, M., Willert, C. and Kompenhans, J. (1998). *Particle Image Velocimetry: A Practical Guide*. Boston, MA: Springer.
Romanuk, T. N., Hayward, A. and Hutchings, J. A. (2011). Trophic level scales positively with body size in fishes. *Glob. Ecol. Biogeogr.* **20**, 231-240.
Satterthwaite, F. E. (1946). An approximate distribution of estimates of variance components. *Biometrics Bull.* **2**, 110-114.
Skorczewski, T., Cheer, A. Y. and Wainwright, P. C. (2012). The benefits of planar circular mouths on suction feeding performance. *J. R. Soc. Interface* **9**, 1767-1773.
Staab, K. L., Holzman, R., Hernandez, L. P. and Wainwright, P. C. (2012). Independently evolved upper jaw protrusion mechanisms show convergent hydrodynamic function in teleost fishes. *J. Exp. Biol.* **215**, 1456-1463.
Stewart, W. J., Cardenas, G. S. and McHenry, M. J. (2013). Zebrafish larvae evade predators by sensing water flow. *J. Exp. Biol.* **216**, 388-398.
Stinson, C. M. and Deban, S. M. (2017). Functional trade-offs in the aquatic feeding performance of salamanders. *Zoology* **125**, 69-78.
Stoner, A. W. and Livingston, R. J. (1984). Ontogenetic patterns in diet and feeding morphology in sympatric sparid fishes from seagrass meadows. *Copeia* **1984**, 174-187.
Svanbäck, R., Wainwright, P. C. and Ferry-Graham, L. A. (2002). Linking cranial kinematics, buccal pressure, and suction feeding performance in largemouth bass. *Physiol. Biochem. Zool.* **75**, 532-543.
Sveen, J. K. (2004). An introduction to MatPIV v. 1.6.1. *Mech. Appl. Math.* **2**, 1-27.
Taylor, Z. J., Gurka, R. and Liberzon, A. (2014). Particle Image Velocimetry for biological mechanics. In *Handbook of Imaging in Biological Mechanics* (ed. C. P. Neu and G. M. Genin), pp. 173-184. Boca Raton, FL: CRC Press.
Trippel, E. A., Kjesbu, O. S. and Solemdal, P. (1997). Effects of adult age and size structure on reproductive output in marine fishes. In *Early Life History and Recruitment in Fish Populations* (ed. R. C. Chambers and E. A. Trippel), pp. 31-62. Dordrecht: Springer Netherlands.
van Leeuwen, J. L. and Muller, M. (1984). Optimum sucking techniques for predatory fish. *Trans. Zool. Soc. London* **37**, 137-169.
Van Wassenbergh, S. and Aerts, P. (2009). Aquatic suction feeding dynamics: insights from computational modelling. *J. R. Soc. Interface* **6**, 149-158.
Van Wassenbergh, S. and Heiss, E. (2016). Phenotypic flexibility of gape anatomy fine-tunes the aquatic prey-capture system of newts. *Sci. Rep.* **6**, 1-8.
Van Wassenbergh, S., Aerts, P. and Herrel, A. (2006a). Hydrodynamic modelling of aquatic suction performance and intra-oral pressures: limitations for comparative studies. *J. R. Soc. Interface* **3**, 507-514.
Van Wassenbergh, S., Aerts, P. and Herrel, A. (2006b). Scaling of suction feeding performance in the catfish *Clarias gariepinus*. *Physiol. Biochem. Zool.* **79**, 43-56.
Van Wassenbergh, S., Herrel, A., Adriaens, D. and Aerts, P. (2007). No trade-off between biting and suction feeding performance in clariid catfishes. *J. Exp. Biol.* **210**, 27-36.
Wainwright, P. C. (2001). Evaluating the use of ram and suction during prey capture by cichlid fishes. *J. Exp. Biol.* **204**, 3039-3051.

Wainwright, P. C. and Bellwood, D. R. (2002). Ecomorphology of feeding in coral reef fishes. In *Coral Reef Fishes: Dynamics and Diversity in a Complex Ecosystem* (ed. P. F. Sale), pp. 33-55. San Diego, CA: Academic Press.
Wainwright, P. C. and Day, S. W. (2007). The forces exerted by aquatic suction feeders on their prey. *J. R. Soc. Interface* **4**, 553-560.
Wainwright, P. C., Ferry-Graham, L. A., Waltzek, T. B., Carroll, A. M., Darrin Hulsey, C. and Grubich, J. R. (2001). Evaluating the use of ram and suction during prey capture by cichlid fishes. *J. Exp. Biol.* **204**, 3039-3051.
Wainwright, P. C., Carroll, A. M., Collar, D. C., Day, S. W., Higham, T. E. and Holzman, R. (2007). Suction feeding mechanics, performance, and diversity in fishes. *Integr. Comp. Biol.* **47**, 96-106.
Weihs, D. (1980). Hydrodynamics of suction feeding of fish in motion. *J. Fish Biol.* **16**, 425-433.
Werner, E. E. (1974). The fish size, prey size, handling time relation in several sunfishes and some implications. *J. Fish.* **31**, 1531-1536.
Westneat, M. W. (2005). Skull biomechanics and suction feeding in fishes. *Fish Physiol.* **23**, 29-75.
Yaniv, S., Elad, D. and Holzman, R. (2014). Suction feeding across fish life stages: flow dynamics from larvae to adults and implications for prey capture. *J. Exp. Biol.* **217**, 3748-3757.
Zaret, T. M. and Kerfoot, W. C. (1975). Fish predation on *Bosmina longirostris*: body-size selection versus visibility selection. *Ecology* **56**, 232-237.

Table S1: The 14 aquatic suction feeding species used in this study, their typical habitat and diet (Froese, R. and Pauly, D. (2017). FishBase.). Values for standard length (SL), gape diameter, time to peak gape (TTPG), peak flow speed (Peak FS) and number of individuals (N) pertain to the specimens used in this study.

Species	**Habitat**	**Diet**	**SL (mm)**	**Gape diameter (mm)**	**TTPG (s)**	**Peak FS (mm/s)**	**N**
Ambystoma tigrinum	Freshwater; vernal pools and other seasonal ponds and stock ponds with low flow.	Feeds on small prey such as worms, insects, and small fish	180-231 (TL)	8.0-18.3	0.015-0.049	219.9-433.7	2
Polypterus endlicheri	Freshwater; inhabits marginal swamps and freshwater lagoons, favors sheltered inshore habitats and muddy regions at the sides of rivers and swampy waters.	Feeds on fishes, insects, crustaceans, molluscs, frogs, plant fragments and seeds.	153-166	5.0-16.1	0.030-0.189	2.7-395.8	2
Danio rerio	Freshwater; slow-moving to stagnant water bodies.	Feeds on worms, small crustaceans and insect larvae	30.1-35.4	1.4-3.02	0.006-0.145	3.9-56.7	5
Carassius auratus	Freshwater; eutrophic waters, well vegetated ponds and canals.	Feeds on plankton, benthic invertebrates, plant material and detritus	205-247	10.9-20.4	0.008-0.109	85.3-622.6	3
Apteronotus albifrons	Freshwater; rapidly flowing waters of creeks with a sandy bottom.	Feeds on insect larvae	65.3-87.3	1.4-4.5	0.003-0.050	1.0-103.5	4
Hemigrammus pulcher	Freshwater; shallow marginal areas, with abundant aquatic macrophytes.	Feeds on insect larvae, winged insects and plant matter	62.7-70.4	3.1-6.3	0.007-0.057	6.7-85.4	5
Pimelodus pictus	Freshwater; upstream parts of rivers, downstream rapids, in backwater zones, on stony bottoms of pools or in trunks.	Feeds on worms, insects, vegetables, and small fish. Omnivorous.	73.6-81.0	3.9-7.4	0.024-0.099	17.7-57.8	3
Nimbochromis venustrus	Freshwater; over sandy substrates in medium to high flowing water.	Feeds on small fish. Piscivorous.	74.8	3.4-7.1	0.048-0.152	13.9-32.8	1
Astronotus ocellatus	Freshwater; quiet shallow waters in mud-bottomed and sand-bottomed canals and ponds	Feeds on small fish, crayfish, worms and insect larvae.	113-142	10.5-20.4	0.008-0.052	39.6-351.1	3

Poecilia sphenops	Freshwater/Brackish; slower flowing regions of coastal sea waters, brackish swamps and freshwater streams	Feeds on worms, crustaceans, insects, plant matter.	58.9	3.0-4.9	0.009- 0.047	9.5-42.1	1
Dascyllus marginatus	Marine; reef-associated, usually in shallow, protected waters in groups	Feeds on zooplankton.	52.6	2.3- 3.9	0.015- 0.057	18.1-110.2	1
Chromis viridis	Marine; reef-associated, large aggregations above thickets of branching corals in shallow, protected waters	Feeds on zooplankton.	44.8-59.1	2.3-4.3	0.008- 0.092	0.8-38.3	2
Chromis pelloura	Marine; reef-associated; in shallow, protected waters	Feeds on zooplankton.	51.3	2.1-3.6	0.030- 0.086	6.1-31.5	1
Lepomis macrochirus	Freshwater; shallow waters of lakes and ponds, slow-moving areas of streams and small rivers preferring deep weed beds	Feeds on snails, small crayfish, insects, worms and small minnows	59.0– 190.0	3.8-21.4	0.004- 0.060	30.4- 485.8	4

Table S2: Slopes of the decay of flow, the distance from the mouth in which flow speed is 7% of total flow, notch angle, and notch area represented as a % of total gape area, estimated for each of the species used in this study.

Species	Slopes of flow decay	Distance of 7% flow (Gape diameters)	Notch angle (°)	Notch area (% of gape area)
Ambystoma tigrinum	-0.77	1.15	139.79	16
Polypterus endlicheri	-0.83	0.98	142.01	6
Danio rerio	-0.93	0.92	140.52	9
Carassius auratus	-0.89	0.95	163.24	4
Apteronotus albifrons	-0.85	0.90	98.97	19
Hemigrammus pulcher	-0.93	0.91	105.59	35
Pimelodus pictus	-0.81	0.97	145.08	14
Nimbochromis venustrus	-0.94	0.90	40.16	73
Astronotus ocellatus	-0.81	1.05	118.10	18
Poecilia sphenops	-0.94	0.93	138.46	18
Dascyllus marginatus	-0.90	0.98	125.45	5
Chromis viridis	-0.92	0.92	113.55	12
Chromis pelloura	-0.89	0.89	110.87	16
Lepomis macrochirus	-0.78	1.04	152.17	5

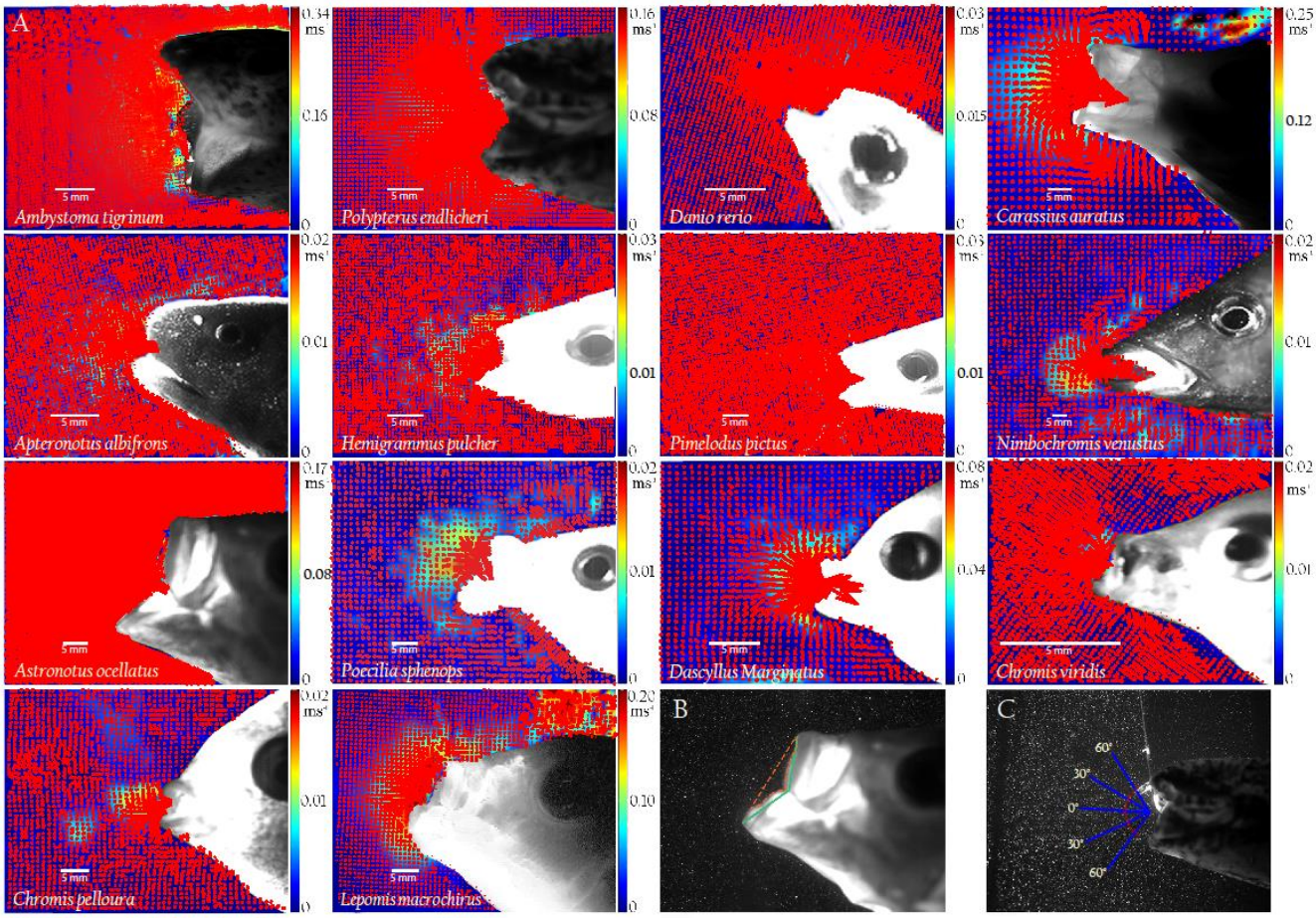

Fig S1: **The diversity of mouth morphology and suction flows across aquatic suction feeders**. (A) Images of fish are overlaid over false color images, depicting faster flows as warmer colors and slower flows as cold colors. Because of an order-of-magnitude difference in peak flow speed, each panel has a different velocity scale. Each figure also shows arrows of the direction of flow with larger arrows representing faster flows. (B) The notch area (orange dash) is defined as the area of the imaginary triangle formed between the projection of the upper jaw, lower jaw, and the intersection point between the maxilla and lower jaw bones. Notch angle (green lines) is defined as the angle between the maxilla and lower jaw bones. (C) Flow speed for each time frame is measured at 13 points (red x markers) located at a distance of ½ gape distance from the mouth center, separated by 10º. The decay of flow speed as a function of the distance from the mouth is characterized based on flow speeds extracted along 5 transects extending from the mouth center outwards (blue lines).